Inorganic Chemistry

Article

pubs.acs.org/IC

Quaternary Pnictides with Complex, Noncentrosymmetric Structures. Synthesis and Structural Characterization of the New Zintl Phases $Na_{11}Ca_2Al_3Sb_8$, $Na_4CaGaSb_3$, and $Na_{15}Ca_3In_5Sb_{12}$

Yi Wang, Stanislav Stoyko, and Svilen Bobev*

Department of Chemistry and Biochemistry, University of Delaware, Newark, Delaware 19716, United States

Supporting Information

ABSTRACT: Three new Zintl phases, $Na_{11}Ca_2Al_3Sb_8$, $Na_4CaGaSb_3$, and $Na_{15}Ca_3In_5Sb_{12}$, have been synthesized by solid-state reactions, and their structures have been determined by single-crystal X-ray diffraction. $Na_{11}Ca_2Al_3Sb_8$ crystallizes with its own structure type (Pearson index *oP*48) with the primitive orthorhombic space group $Pmn2_1$ (No. 31). The structure is best viewed as $[Al_3Sb_8]^{15-}$ units of fused $AlSb_4$ tetrahedra, a novel type of Zintl ion, with Na^+ and Ca^{2+} cations that solvate them. $Na_4CaGaSb_3$ also crystallizes in its own type with the primitive monoclinic space group *Pc* (No. 7; Pearson index *mP*36), and its structure boasts one-dimensional $[GaSb_3]^{6-}$ helical chains of corner-shared $GaSb_4$ tetrahedra. The third new compound, $Na_{15}Ca_3In_5Sb_{12}$, crystallizes with the recently reported $K_2BaCdSb_2$ structure type (space group $Pmc2_1$; Pearson index *oP*12). The $Na_{15}Ca_3In_5Sb_{12}$ structure is based on polyanionic layers made of corner-shared $InSb_4$ tetrahedra. Approximately one-sixth of the In sites are vacant in a statistical manner. All three structures exhibit similarities to the TiNiSi structure type, and the corresponding relationships are discussed. Electronic band structure calculations performed using the tight-binding linear muffin-tin orbital atomic sphere approximation method show small band gaps for all three compounds, which suggests intrinsic semiconducting behavior for these materials.

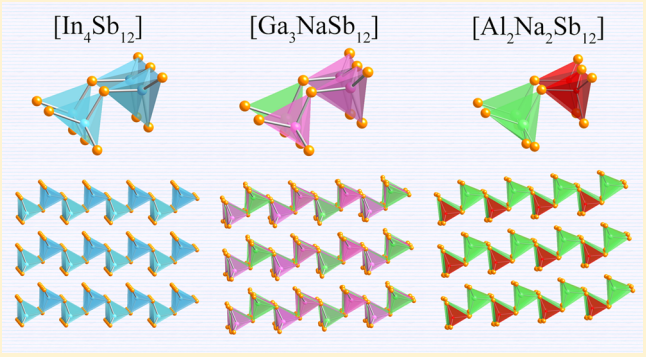

INTRODUCTION

The compounds formed between the alkali or alkaline-earth metals and the post-transition elements from groups 13−15 are typically referred to as Zintl phases.[1,2] Using the Zintl−Klemm concept, the structures of such materials are readily rationalized as cations (less electronegative elements) and anions (more electronegative elements), so that the valence rules are satisfied. Recently, our group has investigated quite a few new cases of presumed Zintl phases, where the cations can be seen as intimately involved in the chemical bonding; for example, $A_{21}Cd_4Sb_{18}$ (A = Eu, Ba),[3] and A_2CdSb_2 (A = Ca, Yb),[4] are two kinds of structures in which the cations proved to be important structure-directing parameters (for the same valence electron count). The series Ba_2ZnPn_2 (Pn = As, Sb, Bi),[5] not surprisingly, demonstrated that for the same structure and valence electron count mixing of the cation and anion states is responsible for the transition from intrinsic semiconducting behavior to metallic behavior as the sizes and electronegativities of the atomic partners are varied. The cited examples are yet another testament to the notion that "closed-shell species", "electron donors/acceptors", "space fillers", etc., which are traditional terminology in the Zintl−Klemm concept, are somewhat far from reality.

The previous work motivated us to extend our research and to seek more new structures with complex bonding characteristics. The fact that in recent years many ternary antimonides have gained interest as prospective materials for applications in thermoelectric energy conversion[6−8] is another reason why we were attracted to the ongoing research efforts in this general area. Herein, we report the results from a new direction of this project, which includes the identification and the characterization of three new Zintl phases: $Na_{11}Ca_2Al_3Sb_8$, $Na_4CaGaSb_3$, and $Na_{15}Ca_3In_5Sb_{12}$. They provide new examples for the significant role of cations in chemical bonding and structure formation in Zintl phases. The focus of this paper is on the synthesis, the single-crystal X-ray diffraction studies, and the electronic structures [calculated by the tight-binding linear muffin-tin orbital atomic sphere approximation (TB-LMTO-ASA) method[9]] of the three new compounds. The structural similarities among them are presented; the close structural relationship to the TiNiSi structure type (also known as the Co_2Si type[10]) is discussed as well.

EXPERIMENTAL SECTION

Synthesis. Because of the high sensitivity of elemental Na to air and moisture, handling of the starting materials required extreme caution. All manipulations were carried out inside an Ar-filled glovebox

Received: November 25, 2014
Published: February 4, 2015

DOI: 10.1021/ic502822v
Inorg. Chem. 2015, 54, 1931−1939

with a controlled atmosphere or under vacuum. The metals were purchased from Alfa or Aldrich (purity >99.9%) and were used as received. The Na surface was scrapped off with a scalpel blade immediately before use.

Single crystals of the title compounds were first identified from exploratory reactions of the corresponding elements Na, Ca, Tr, and Sb in the molar ratio of 3:3:1:4 (Tr = Triel, i.e., a group 13 element). The metals were weighed in the glovebox (total weight ca. 500 mg) and loaded into Nb tubes, which were then closed by arc welding under high-purity Ar gas. The sealed Nb containers were subsequently jacketed within evacuated fused-silica tubes. The reaction mixtures were heated to 1173 K at a rate of 100 K/h and equilibrated at this temperature for 24 h. Following a cooling step to 773 K at a rate of 5 K/h, the products were brought to room temperature over 12 h. On the basis of analysis of the single-crystal and powder X-ray diffraction data, multiple binary, ternary, and quaternary phases were obtained in each case. Besides $Na_{11}Ca_2Al_3Sb_8$, $Na_4CaGaSb_3$, and $Na_{15}Ca_3In_5Sb_{12}$, we were also able to identify $Na_3Ca_3AlSb_4$,[11] $Ca_5Ga_2Sb_6$,[12] Na_3InSb_2,[13] $Ca_{11}Sb_{10}$,[14] and NaSb,[15] among some other, yet unidentified phases.

After the structures and chemical compositions were established by single-crystal work, new reactions with the proper stoichiometry were loaded. They yielded the desired compounds as major products. The produced samples contained small amounts of impurity phase(s), but the bulk consisted of small, shiny crystals with a dark-metallic luster that were the targeted phases. The materials were brittle and air-sensitive.

We speculated that the three newly identified phases might have isostructural "neighbors" within the arsenides or bismuthides. Such reactions were set up, and the corresponding products were analyzed—no isostructural arsenides or bismuthides were found; instead, we uncovered new phases with different structures, which will be the subject of a forthcoming publication. We also explored periodic trends by changing the alkali and/or alkaline-earth metal and will detail the results from this work in another follow-up article.

Caution! *At the aforementioned conditions, Na metal will evaporate and could create high pressure. It is therefore important to use as long as possible Nb containers ($^3/_8$ in. in diameter and ca. $2^1/_2$ to 3 in. in length) and long fused-silica tubes ($^7/_8$ in. in diameter and ca. 10−12 in. in length), which must be left protruding outside the furnace. Doing so minimizes the risk of serious accidents because, in the case of a leak, the Na vapors will diffuse and condense at the cold end of the fused-silica tube. If this happens, the furnace must be stopped immediately.*

Powder X-ray Diffraction. The as-synthesized samples were ground in the glovebox to fine powders. Then, powder X-ray diffraction patterns were taken at room temperature on a Rigaku MiniFlex powder diffractometer using filtered Cu Kα radiation (λ = 1.54056 Å), also operated inside the glovebox. Data analysis was done using the *JADE 6.5* software package.

Because of the limited capabilities of the MiniFlex, combined with the low symmetry and complex nature of the structures, the patterns had many peaks that could not be well-resolved. Therefore, the powder X-ray diffraction patterns were only used for phase identification; all reported cell parameters were refined by single-crystal X-ray diffraction data.

Single-Crystal X-ray Diffraction. The single-crystal X-ray diffraction experiments were done on a Bruker SMART CCD-based diffractometer with a three-circle goniometer, employing monochromatized Mo Kα radiation (λ = 0.71073 Å). During the data collection, the temperature was kept at 200 K by a cold N_2 stream. Maintaining an inert atmosphere during the experiments was critical because the crystals deteriorate very quickly if exposed to the laboratory air (all preparations were done in a glovebox with an optical microscope and under dried Paratone N oil). Data acquisition and integration were completed using the programs *SMART* and *SAINT*, supplied by Bruker.[16] Semiempirical absorption correction based on equivalent reflections was applied using *SADABS*.[17] The structures were solved by direct methods and refined with a full-matrix least-squares method on F^2, as implemented in *SHELXTL*.[18] The refinements converged readily to low conventional residuals and final difference Fourier maps, which were flat. Refined parameters included the scale factors and atomic positions with the corresponding anisotropic displacement parameters. Where applicable, site occupation factors were also refined. Additional details pertaining to the structure refinements and the way the mixed-occupied sites were handled, as well as structural drawings with anisotropic displacement parameters at the 95% probability level, are provided as Supporting Information (SI).

Selected crystallographic information and refinement parameters for $Na_{11}Ca_2Al_3Sb_8$, $Na_4CaGaSb_{12}$, and $Na_{15}Ca_3In_5Sb_{12}$ are summarized in Table 1. Final positional and equivalent isotropic displacement parameters are given in Tables 2−4. Relevant interatomic distances and angles are listed in Table 5. CIFs are provided as SI; the files have

Table 1. Selected Single-Crystal Data Collection and Structure Refinement Parameters for $Na_{11}Ca_2Al_3Sb_8$, $Na_4CaGaSb_3$, and $Na_{15}Ca_3In_5Sb_{12}$

empirical formula[a]	$Na_{11}Ca_2Al_3Sb_8$	$Na_4CaGaSb_3$	$Na_5CaIn_{1.66}Sb_2$
fw	1387.99	567.01	833.78
temperature (K)		200(2)	
radiation, λ (Å)		Mo Kα, 0.71073	
space group	$Pmn2_1$ (No. 31)	Pc (No. 7)	$Pmc2_1$ (No. 26)
Z	2	4	1
a (Å)	18.9690(15)	9.1513(9)	4.7609(5)
b (Å)	8.8533(7)	8.9852(9)	9.1680(10)
c (Å)	7.9304(7)	12.2305(12)	7.8898(8)
β (deg)		97.840(1)	
V (Å^3)	1331.8(2)	996.3(2)	344.37(6)
ρ_{cal} (g/cm^3)	3.46	3.78	4.02
μ (cm^{-1})	86.4	113.3	109.6
GOF on F^2	1.051	0.994	1.106
Flack parameter	0.02(4)	0.04(1)	0.08(9)
unique reflns	3716	5260	1058
refined param	119	165	38
R1 [$I > 2\sigma(I)$][b]	0.0288	0.0210	0.0301
wR2 [$I > 2\sigma(I)$][b]	0.0598	0.0411	0.0617

[a]Refined formulas with freely refined occupancies of the Na/Ca mixed positions: $Na_{10.90(2)}Ca_{2.10}Al_3Sb_8$, $Na_{3.98(1)}Ca_{1.02}GaSb_3$, and $Na_{5.06(2)}Ca_{0.94}In_{1.58(2)}Sb_2$, respectively. [b]R1 = $\sum||F_o| - |F_c||/\sum|F_o|$; wR2 = $[\sum[w(F_o^2 - F_c^2)^2]/\sum[w(F_o^2)^2]]^{1/2}$, where $w = 1/[\sigma^2F_o^2 + (AP)^2 + (BP)]$, and $P = (F_o^2 + 2F_c^2)/3$; A, B = weight coefficients.

Table 2. Atomic Coordinates and Equivalent Isotropic Displacement Parameters U_{eq}[a] for $Na_{11}Ca_2Al_3Sb_8$

atom	site	x	y	z	U_{eq} (Å^2)
Na1/Ca1[b]	4b	0.7560(1)	0.9466(2)	0.9845(2)	0.0245(4)
Na2	4b	0.8817(2)	0.5935(4)	0.9494(5)	0.0377(7)
Na3	4b	0.7499(2)	0.6654(3)	0.6288(4)	0.0286(7)
Na4	4b	0.6307(2)	0.5715(4)	0.9546(4)	0.0341(7)
Na5	4b	0.6242(1)	0.8027(3)	0.3255(4)	0.0289(7)
Na6	2a	0	0.9484(4)	0.0000(5)	0.0264(8)
Na7	2a	0	0.3384(4)	0.1289(6)	0.0285(9)
Ca2	2a	0	0.0809(2)	0.4897(3)	0.0284(5)
Al1	4b	0.8772(1)	0.8351(2)	0.3371(3)	0.0207(4)
Al2	2a	0	0.6862(3)	0.6153(4)	0.0199(6)
Sb1	4b	0.8852(1)	0.8633(1)	0.6853(1)	0.0208(1)
Sb2	4b	0.7309(1)	0.3311(1)	0.7350(1)	0.0242(1)
Sb3	4b	0.6265(2)	0.8778(1)	0.7205(1)	0.0201(1)
Sb4	2a	0	0.6814(1)	0.2679(1)	0.0197(1)
Sb5	2a	0	0.4016(1)	0.7268(1)	0.0215(1)

[a]U_{eq} is defined as one-third of the trace of the orthogonalized U_{ij} tensor. [b]Refined freely as 55(1)% Ca and 45% Na; in the final refinement model, for simplicity, constrained to 50% Ca and 50% Na.

DOI: 10.1021/ic502822v
Inorg. Chem. 2015, 54, 1931−1939

Table 3. Atomic Coordinates and Equivalent Isotropic Displacement Parameters U_{eq}[a] for $Na_4CaGaSb_3$

atom	site	x	y	z	U_{eq} (Å^2)
Na1/Ca1[b]	2a	0.0000(2)	0.9406(2)	0.0001(1)	0.0207(3)
Na2/Ca2[c]	2a	0.6808(1)	0.9585(2)	0.6713(1)	0.0182(3)
Na3	2a	0.9566(3)	0.8047(2)	0.2811(2)	0.0263(5)
Na4	2a	0.9153(2)	0.6726(2)	0.5412(2)	0.0236(5)
Na5	2a	0.8502(3)	0.6032(3)	0.8155(2)	0.0346(6)
Na6	2a	0.5697(2)	0.3371(2)	0.7297(2)	0.0275(5)
Na7	2a	0.5443(2)	0.5925(3)	0.5054(2)	0.0286(5)
Na8	2a	0.2392(2)	0.6631(2)	0.8959(2)	0.0248(5)
Na9	2a	0.2021(3)	0.4396(3)	0.6606(2)	0.0418(6)
Ca3	2a	0.3427(1)	0.0471(1)	0.8451(1)	0.0184(2)
Ga1	2a	0.5977(1)	0.8254(1)	0.9572(1)	0.0176(1)
Ga2	2a	0.2770(1)	0.8274(1)	0.6249(1)	0.0170(1)
Sb1	2a	0.8087(1)	0.3456(1)	0.5671(1)	0.0206(1)
Sb2	2a	0.6897(1)	0.8937(1)	0.4131(1)	0.0151(1)
Sb3	2a	0.5012(1)	0.6875(1)	0.7601(1)	0.0176(1)
Sb4	2a	0.3573(1)	0.8778(1)	0.0831(1)	0.0145(1)
Sb5	2a	0.2093(1)	0.6650(1)	0.4413(1)	0.0183(1)
Sb6	2a	0.0430(1)	0.8705(1)	0.7380(1)	0.0162(1)

[a]U_{eq} is defined as one-third of the trace of the orthogonalized U_{ij} tensor. [b]Refined freely as 60(1)% Ca and 40% Na; in the final refinement model, for simplicity, constrained to 60% Ca and 40% Na. [c]Refined freely as 37(1)% Ca and 63% Na; in the final refinement model, for simplicity, constrained to 40% Ca and 60% Na.

Table 4. Atomic Coordinates and Equivalent Isotropic Displacement Parameters U_{eq}[a] for $Na_{15}Ca_3In_5Sb_{12}$

atom	site	x	y	z	U_{eq} (Å^2)
Na1	2b	1/2	0.4152(5)	0.0489(6)	0.036(1)
Na2	2a	0	0.3262(5)	0.3630(6)	0.027(1)
Na3/Ca3[b]	2a	0	0.0613(4)	0.0000(4)	0.0215(6)
In	2b	1/2	0.1786(1)	0.6558(1)	0.0234(2)
Sb1	2b	1/2	0.1197(1)	0.2868(1)	0.0180(1)
Sb2	2a	0	0.6559(1)	0.2618(1)	0.0344(2)

[a]U_{eq} is defined as one-third of the trace of the orthogonalized U_{ij} tensor. [b]Refined freely as 53(1)% Ca and 47% Na; in the final refinement model, for simplicity, constrained to 50% Ca and 50% Na.

also been deposited with Fachinformationszentrum Karlsruhe, 76344 Eggenstein-Leopoldshafen, Germany [fax (49) 7247-808-666; e-mail crysdata@fiz.karlsruhe.de] with depository numbers CSD 428753 for $Na_{11}Ca_2Al_3Sb_8$, CSD 428754 for $Na_4CaGaSb_3$, and CSD 428752 for $Na_{15}Ca_3In_5Sb_{12}$.

Energy-Dispersive X-ray Spectroscopy (EDX). To verify the refined compositions, selected single crystals from each sample were subjected to EDX analysis. A JEOL 7400 F electron microscope, equipped with an Oxford INCA spectrometer, was employed. The analyses were severely hindered by the air sensitivity of the studied samples, and the obtained data could only confirm the elemental makeup; no quantitative interpretation of the results was possible.

Electronic Structure Calculations. The electronic structure calculations were carried out with the TB-LMTO method[9] using the *LMTO47* program.[19−21] The total and partial density of states (DOS) and crystal orbital Hamilton population (COHP)[22] curves of selected interactions are presented and discussed. Exchange and correlation terms were treated by the local density approximation.[23] All relativistic effects except spin−orbit coupling were taken into account by using a scalar relativistic approximation. The basis sets including 3s, 3p, and 3d orbitals for Na and Al, 4s, 4p, and 3d orbitals for Ca and Ga, and 5s, 5p, 5d, and 4f orbitals for In and Sb were treated by the Löwdin downfolding technique.[24] The *k*-space integrations were conducted using the tetrahedron method,[25] and the Fermi level was set at 0 eV as the energy reference.

RESULTS AND DISCUSSION

Structure and Chemical Bonding of $Na_{15}Ca_3In_5Sb_{12}$. We begin our discussion on the chemical bonding by describing the structure of $Na_{15}Ca_3In_5Sb_{12}$, which is the simplest among the three (Figure 1a). $Na_{15}Ca_3In_5Sb_{12}$ appears to be the first structurally characterized compound in the quaternary Na−Ca−In−Sb phase diagram; it crystallizes in the orthorhombic space group $Pmc2_1$ (Pearson index *oP*12).

$Na_{15}Ca_3In_5Sb_{12}$ (i.e., $Na_2(Na_{0.5}Ca_{0.5})In_{0.83}Sb_2$) is best described as a substitution derivative of the recently reported Zintl phase $K_2BaCdSb_2$,[26] whereby the trivalent In (partially occupied) takes the role of the divalent Cd.[27] Because the important features of this structure have already been discussed,[26] in the following paragraphs we will focus on a few details and on the structural relationship to the other two compounds.

There are six crystallographically unique atoms in the asymmetric unit (Table 2), which include two Na sites, one mixed-occupied Ca/Na site, one In site, and two Sb sites. The In site, as mentioned already (and elaborated on in the SI), is not fully occupied, with one-sixth of the positions being randomly vacant. When the disorder is ignored, the structure can be described as infinite $[InSb_2]^{2-}$ polyanionic layers made of corner-shared $InSb_4$ tetrahedra (Figures 1a, 2a, and S3 in the SI). Defects in the polyanions of the Zintl phases are rare but not without precedent, as demonstrated on the example of $Eu_5Cd_3Sb_6$.[28] In the latter structure (own type), one-fourth of the Cd positions are randomly vacant.

There are no direct homoatomic interactions. The In−Sb distances range from 2.924(7) to 2.960(8) Å (Table 5). Within the tetrahedra, the Sb−In−Sb angles range from 100.18(3)° to 112.41(2)°, attesting to a slight distortion from the ideal tetrahedral geometry. The numerical values for the In−Sb bonds and Sb−In−Sb angles compare well with those reported for other ternary A−In−Sb phases (A = alkali or alkaline-earth metal), such as $Ca_5In_2Sb_6$[29] and Na_3InSb_2.[13] The In−Sb interatomic distances (Table 5) are only ca. 4−6% longer than the sum of their single-bonded Pauling radii (e.g., $r_{In} + r_{Sb}$ = 1.421 + 1.391 = 2.812 Å),[30] suggesting appreciable covalent bonding between them.

The structure also contains Na^+ and Ca^{2+} cations, which fill the space between the polyanionic layers. As discussed in a previous paper,[26] following the Zintl−Klemm concept,[1,2] the parent $K_2BaCdSb_2$ structure can be rationalized as $(K^+)_2(Ba^{2+})(Cd^{2+})(Sb^{3-})_2$. In the same manner, taking into account the disorder, $Na_{15}Ca_3In_5Sb_{12}$ can also be viewed as a Zintl phase, the formula of which can be expressed as $(Na^+)_{15}(Ca^{2+})_3(In^{3+})_5(Sb^{3-})_{12}$. This argument is nicely supported by the electronic structure calculations, which show opening of a band gap right at the energy where the bonding interactions are optimized (vide infra).

Structure and Chemical Bonding of $Na_4CaGaSb_3$. Upon replacement of the heavier In with the lighter and smaller Ga, the same reaction scheme that produced $Na_{15}Ca_3In_5Sb_{12}$ allowed for the quantitative synthesis of the new phase $Na_4CaGaSb_3$ (=$Na_{16}Ca_4Ga_4Sb_{12}$). As can be inferred from the close compositions, the two structures are similar, although there are distinct differences. The structure is projected in Figure 1b; some important similarities and

DOI: 10.1021/ic502822v
Inorg. Chem. 2015, 54, 1931−1939

Table 5. Selected Interatomic Distances (Å) and Angles (deg) in $Na_{11}Ca_2Al_3Sb_8$, $Na_4CaGaSb_3$, and $Na_{15}Ca_3In_5Sb_{12}$

$Na_{11}Ca_2Al_3Sb_8$		$Na_4CaGaSb_3$		$Na_{15}Ca_3In_5Sb_{12}$	
Al1−Sb2	2.650(2)	Ga1−Sb1	2.6812(7)	In−Sb1	2.924(1)
Al1−Sb3	2.706(2)	Ga1−Sb2	2.7374(7)	In−Sb2 (×2)	2.9436(8)
Al1−Sb4	2.753(2)	Ga1−Sb3	2.7461(7)	In−Sb1	2.961(1)
Al1−Sb1	2.777(2)	Ga1−Sb4	2.8913(7)	Na2−Sb1 (×2)	3.101(3)
Al2−Sb5	2.670(3)	Ga2−Sb5	2.6792(7)	Na2−Sb2	3.127(5)
Al2−Sb1 (×2)	2.739(1)	Ga2−Sb6	2.7310(7)	Na2−Sb2	3.150(5)
Al2−Sb4	2.756(3)	Ga2−Sb3	2.7568(7)		
Na5−Sb5	3.071(3)	Ga2−Sb4	2.8142(7)		
Na5−Sb2	3.078(3)	Na3−Sb5	3.086(2)		
Na5−Sb1	3.165(3)	Na3−Sb6	3.087(2)		
Na5−Sb3	3.202(3)	Na3−Sb1	3.089(2)		
Na7−Sb3 (×2)	3.154(3)	Na3−Sb2	3.207(2)		
Na7−Sb4	3.230(4)				
Na7−Sb5	3.238(4)				
Sb1−Al1−Sb2	113.44(7)	Sb1−Ga1−Sb2	114.02(7)	Sb1−In−Sb1	100.18(3)
Sb1−Al1−Sb3	104.95(7)	Sb2−Ga1−Sb3	108.31(2)	Sb2−In−Sb2	107.94(4)
Sb1−Al1−Al4	101.32(7)	Sb3−Ga1−Sb4	111.35(2)	Sb1−In−Sb2	112.41(2)
Sb2−Al1−Sb3	113.39(8)	Sb1−Ga1−Sb4	111.98(3)	Sb2−In−Sb1	111.93(2)
Sb2−Al1−Sb4	108.53(9)	Sb1−Ga1−Sb3	107.74(6)		
Sb3−Al1−Sb4	114.58(6)	Sb2−Ga1−Sb4	103.39(2)		
Sb1−Al2−Sb1	105.45(2)	Sb3−Ga2−Sb4	110.28(2)		
Sb1−Al2−Sb4	102.22(5)	Sb3−Ga2−Sb5	108.83(2)		
Sb1−Al2−Sb5	118.22(7)	Sb3−Ga2−Sb6	109.36(4)		
Sb4−Al2−Sb5	108.22(6)	Sb4−Ga2−Sb5	113.38(3)		
		Sb4−Ga2−Sb6	101.58(4)		
		Sb5−Ga2−Sb6	103.20(4)		

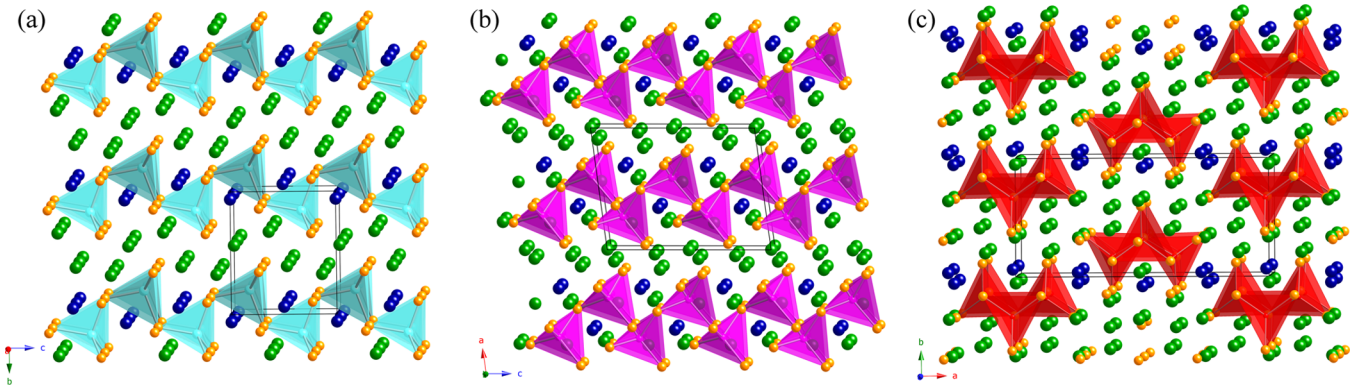

Figure 1. Polyhedral views of the structures of $Na_{15}Ca_3In_5Sb_{12}$ (a), $Na_4CaGaSb_3$ (b), and $Na_{11}Ca_2Al_3Sb_8$ (c). The common atoms—Ca, Na, and Sb—are drawn as blue, green, and orange spheres, respectively. The atoms centering the Sb tetrahedra—In, Ga, and Al—are shown in light blue, pink, and red, respectively.

differences between $Na_{15}Ca_3In_5Sb_{12}$ and $Na_4CaGaSb_3$ are shown in Figures 2 and S5 in the SI.

$Na_4CaGaSb_3$ crystallizes in its own structure type with the primitive monoclinic space group *Pc* (Pearson symbol *mP*36). The structure contains eight Na, two Ca, two Ga, and six Sb atoms in the asymmetric unit. In analogy to what we already discussed for $Na_{15}Ca_3In_5Sb_{12}$, the two Ca sites here are also mixed-occupied (Table 3). The $Na_4CaGaSb_3$ structure can be viewed as one-dimensional $[GaSb_3]^{6-}$ helical chains made up of corner-shared $GaSb_4$ tetrahedra (Figure 2b). The chains propagate along the crystallographic *c* direction, with Na and Ca cations filling the space between them. Importantly, if one considers some of the Na cations, Na3 in the current nomenclature, as part of the polyanionic structure (vide infra), hypothetical $[Ga_{2/3}Na_{1/3}Sb_2]$ layers of corner-shared $GaSb_4$ and $NaSb_4$ tetrahedra can be derived (Figure S5 in the SI). Such hybrid layers would have the same topology as the previously described $[InSb_2]$ layers made solely of corner-shared $InSb_4$ tetrahedra.

The corresponding Ga−Sb distances range from 2.679(3) to 2.891(5) Å (Table 5). The range is somewhat wider than expected, and the sum of the Pauling single-bonded radii (e.g., $r_{Ga} + r_{Sb} = 1.246 + 1.391 = 2.637$ Å)[30] confirms that there will be significant variations in the Ga−Sb bonding.[31] The Sb−Ga−Sb angles, which range from 101.58(4)° to 114.02(7)°, also indicate that the $GaSb_4$ tetrahedra are somewhat more distorted than the aforementioned $InSb_4$ tetrahedra, which could be a subtle feature of the Ga−Sb bonding. It appears the former speculation is more likely because this observation is not unprecedented; other ternary A−Ga−Sb phases, such as

DOI: 10.1021/ic502822v
Inorg. Chem. 2015, 54, 1931−1939

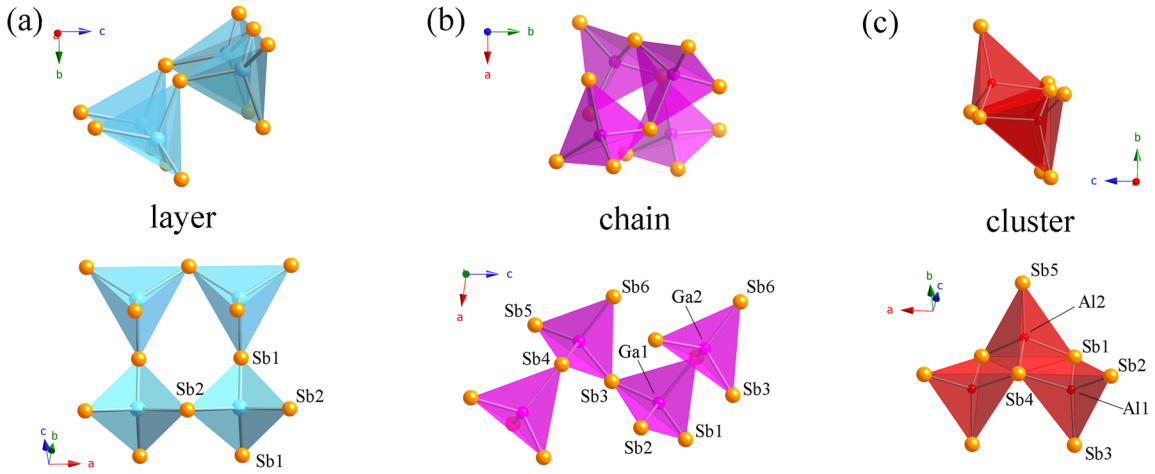

Figure 2. Detailed drawings in different orientations of a $[In_4Sb_{12}]$ cutout from the layers of the $Na_{15}Ca_3In_5Sb_{12}$ structure (a), a $[Ga_4Sb_{13}]$ cutout from the chains in the $Na_4CaGaSb_3$ structure (b), and the $[Al_3Sb_8]$ cluster in the $Na_{11}Ca_2Al_3Sb_8$ structure (c). The atoms are labeled, and the relevant distances and angles are listed in Table 5

$Ca_5Ga_2Sb_6$[12] and $Na_2Ga_3Sb_3$,[32] whose structures are also based on $GaSb_4$ tetrahedra, show a comparatively wide range of Ga−Sb distances. Just like $Ca_5Ga_2Sb_6$[12] and $Na_2Ga_3Sb_3$,[32] the new compound $Na_4CaGaSb_3$ is also a Zintl phase, which can be rationalized as $(Na^+)_4Ca^{2+}Ga^{3+}(Sb^{3-})_3$.

Structure and Chemical Bonding of $Na_{11}Ca_2Al_3Sb_8$. The last, and the most dimensionally reduced, structure of all three is that of $Na_{11}Ca_2Al_3Sb_8$. This new compound crystallizes with the noncentrosymmetric orthorhombic space group $Pmn2_1$ (Figures 1c and S1 in the SI). Inspection of *Pearson's Handbook*[10] and the Inorganic Crystals Structure Database (ICSD)[33] reveals that there is no precedent of a structure with the same sequence of Wyckoff letters, suggesting that the $Na_{11}Ca_2Al_3Sb_8$ structure represents yet another novel structure type (Pearson symbol *oP*48). The structure contains six Na, two Ca, two Al, and five Sb atoms in the asymmetric unit. One of the two Ca sites here is mixed-occupied also (Table 2).

As emphasized in Figure 2c, the most prominent feature of this structure is the $[Al_3Sb_8]^{15-}$ subunit. This molecular-like fragment is first-of-a-kind in the chemistry of the Zintl phases and ions[1,2] and is built of three $AlSb_4$ tetrahedra, which share edges with each other in a *cis*-arrangement. The trimers are composed of two tetrahedra that are crystallographically unique; the third one is a symmetry-equivalent image, generated by the mirror plane perpendicular to the *a* direction and passing through the Al atom #2. All Al−Sb distances fall in the range of 2.650(2)−2.777(2) Å (Table 5). The range is much narrower than the interval observed for the Ga−Sb distances in $Na_4CaGaSb_3$ (vide supra), and the numerical values match well with the sum of the corresponding Pauling radii (e.g., $r_{Al} + r_{Sb}$ = 1.248 + 1.391 = 2.639 Å).[30] The Sb−Al−Sb angles vary from 101.32(7)° to 118.22(7)°. All structural metrics compare well with those reported for other structures based on $AlSb_4$ tetrahedra, for instance, $Ca_5Al_2Sb_6$[34] and $Na_7Al_2Sb_5$.[35] Given the absence of homoatomic interactions, $Na_{11}Ca_2Al_3Sb_8$ can also be classified as a Zintl phase based on the formulation $(Na^+)_{11}(Ca^{2+})_2(Al^{3+})_3(Sb^{3-})_8$.

Structural Relationships. Having discussed the important features of the three structures, we now turn our attention to the structural relationships among them. Briefly, let us recall that $Na_{15}Ca_3In_5Sb_{12}$ boasts two-dimensional $[InSb_2]^{2-}$ polyanionic layers of corner-shared $InSb_4$ tetrahedra (again, not considering the vacant In sites that could account for ribbons if long-range-ordered), $Na_4CaGaSb_3$ features one-dimensional $[GaSb_3]^{6-}$ helical chains of $GaSb_4$ tetrahedra, and $Na_{11}Ca_2Al_3Sb_8$ has trimeric $[Al_3Sb_8]^{15-}$ zero-dimensional fragments of fused $AlSb_4$ tetrahedra.

At first glance, there is no connection between the three structures. However, after careful consideration, striking similarities among the three compounds become apparent upon studying the cations' coordination. For example, one can see that in the three structures there are two types of Na atoms: interlayer and intralayer Na atoms, i.e., the atoms residing *between* and *within* the layers, respectively. The nuances of the interlayer and intralayer bonding, and the subtly different roles the two types of cations play, have already been discussed on the examples of $Ba_3Cd_2Sb_4$ and its Sr-substituted variant $Ba_{3-x}Sr_xCd_2Sb_4$.[36] This discussion was subsequently extended along the lines of the coloring of the cation sites by cations with different charges, as in $K_2BaCdSb_2$,[26] which is the prototype of the herein-presented $Na_{15}Ca_3In_5Sb_{12}$. In the $Na_4CaGaSb_3$ and $Na_{11}Ca_2Al_3Sb_8$ structures, which are not layered per se, the "intralayer" Na atoms will be those located beside the $[GaSb_3]^{6-}$ helical chains or the $[Al_3Sb_8]^{15-}$ trimers. In Figure 3a, the Na2 atom is shown as surrounded by four Sb atoms in distorted tetrahedral geometry and is positioned between two adjacent helical chains, connecting them by Na−Sb bonds. In Figure 3b, Na5 in the $Na_{11}Ca_2Al_3Sb_8$ structure is shown in its tetrahedral coordination of four Sb atoms. Two such tetrahedra form a dimer, which is connected to surrounding Al_3Sb_8 trimers.

Clearly, the common denominator here is the ability of these Na atoms to participate in covalent-like bonding with the polyanions. In both structures, the intralayer Na is tetrahedrally coordinated with the Na−Sb bonds showing "normal" distances. The Na−Sb distances range from 3.086(2) to 3.207(2) Å in $Na_4CaGaSb_3$ and from 3.078(3) to 3.202(3) Å in $Na_{11}Ca_2Al_3Sb_8$, respectively. The range is similar to the reported distances in $Na_2YbCdSb_2$ (ordered quaternary variant of the Yb_2CdSb_2 structure), where the tetrahedral Na is located ca. 3.1 Å away from its closest neighbors.[26] In another structure type, adopted by at least five more Zintl phases $KA_2Cd_2Sb_3$ (A = Ca, Sr, Ba, Eu, Yb),[37] all K cations are in tetrahedral coordination also, which is not common for such a large ion;

DOI: 10.1021/ic502822v
Inorg. Chem. 2015, 54, 1931−1939

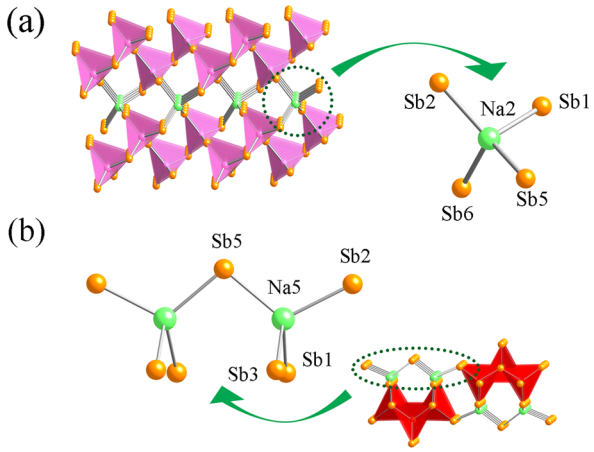

Figure 3. Polyanionic substructures of $Na_4CaGaSb_3$ (a) and $Na_{11}Ca_2Al_3Sb_8$ (b) viewed as tetrahedral "hybrid layers", made up of Ga, Na, Sb and Al, Na, Sb, respectively. The atoms are labeled, and the relevant distances are listed in Table 5

they are also tightly coordinated with K−Sb distances as short as 3.36 Å.[37] All of the above-mentioned interatomic distance match well with the sum of the corresponding Pauling single-bonded radii (e.g., $r_{Na} + r_{Sb}$ = 1.572 + 1.391 = 2.963 Å; $r_K + r_{Sb}$ = 2.025 + 1.391 = 3.416 Å).

Including the intralayer Na atoms in the consideration of the polyanions in $Na_4CaGaSb_3$ and $Na_{11}Ca_2Al_3Sb_8$, one can notice that they can be viewed as "hybrid-layered" structures (Figure 4). For the $Na_4CaGaSb_3$ structure, the ratio of Ga/Na is 2:1 within the "hybrid layers", while in $Na_{11}Ca_2Al_3Sb_8$, the ratio of Al/Na is 1:1. In the $Na_{15}Ca_3In_5Sb_{12}$ structure, the $^2_\infty[InSb_2]$ layers are "free-standing"; i.e., the Na atoms here are positioned between adjacent layers (see the SI).

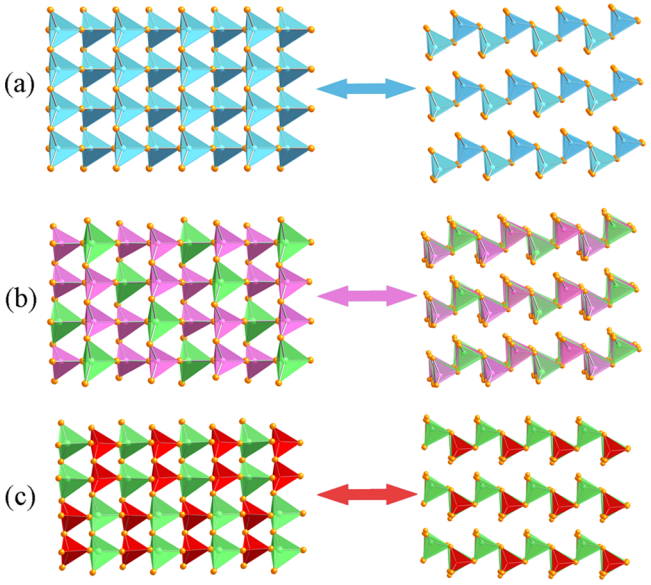

Figure 4. Structural relationships among $Na_{15}Ca_3In_5Sb_{12}$, $Na_4CaGaSb_3$, and $Na_{11}Ca_2Al_3Sb_8$. Panel a shows the idealized, defect-free $[InSb_2]$ polyanionic layers in $Na_{15}Ca_3In_5Sb_{12}$; panel b depicts the hypothetical hybrid $[Ga_{2/3}Na_{1/3}Sb_2]$ layers in $Na_4CaGaSb_3$; panel c shows the imaginary $[Al_{1/2}Na_{1/2}Sb_2]$ layers in $Na_{11}Ca_2Al_3Sb_8$. In all drawings, two different orientations are shown, with the tetrahedra rendered in green corresponding to the $NaSb_4$ units.

The participation of different amounts of Na atoms in the formation of "hybrid polyanionic layers" could also explain the variations of the Ga−Sb and Al−Sb bond lengths. As we discussed before, the shortest Ga−Sb bond measures 2.679(3) Å (between Ga2 and Sb5). The second shortest is 2.681(6) Å between Ga1 and Sb1 (Table 5). Considering the proximity of the intralayer Na2 atom, which impacts both Ga1 and Ga2 through Sb1 and Sb5, respectively, we can argue that the corresponding Ga−Sb distances ought to be on the short side in order for the structure to "make room" for the more spatially demanding Na. In the $Na_{11}Ca_2Al_3Sb_8$ structure, the shortest Al−Sb bond is 2.650(2) Å and also occurs in the $[Al_2Na_2Sb_{12}]$ subunit (Figure S4 in the SI) between Al1 and Sb2 (Table 5). Here, Na5 is affecting Al1 through the Sb2 vertex (Figure 3). In analogy with the $[Ga_3NaSb_{12}]$ fragment (Figure S4 in the SI), it is again reasonable to expect that Al1−Sb1 will be "squeezed" and would be the shortest bond with the $AlSb_4$ tetrahedra.

Relationship to the Common TiNiSi Structure Type. A different description of these structures can be proposed on the basis of their close relationship with the ubiquitous TiNiSi structure type (also referred to as the Co_2Si structure type).[10] The compound $Na_3In_2Bi_3$ $[NaIn_{0.67}Bi = (Na^+)(In^{3+})_{0.67}(Bi^{3-})]$[38] is known to form with this structure (Figure 5a), and it can be described as a polyanionic InBi framework

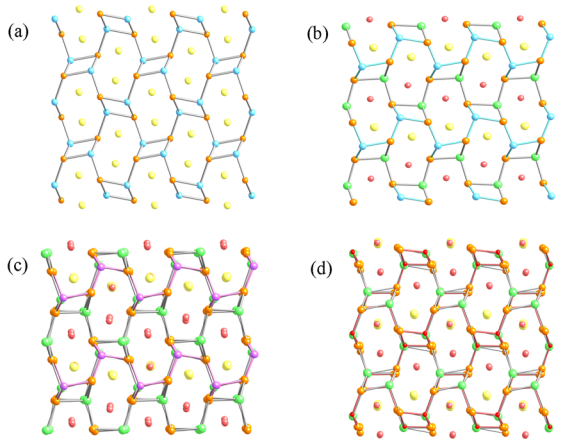

Figure 5. Structural relationships among $Na_3In_2Bi_3$ (TiNiSi structure type)[36] and $Na_{15}Ca_3In_5Sb_{12}$, $Na_4CaGaSb_3$, and $Na_{11}Ca_2Al_3Sb_8$. Panel a shows the three-dimensional framework of the parent structure with Na shown in yellow, In shown in blue, and Bi shown in orange. Panels b−d depict the structures of $Na_{15}Ca_3In_5Sb_{12}$, $Na_4CaGaSb_3$, and $Na_{11}Ca_2Al_3Sb_8$, where the frameworks include the tetrahedrally coordinated Na atoms. To guide the eye, the In−Sb, Ga−Sb, and Al−Sb bonds are colored with the respective elemental colors—blue, pink, and red—and the Na−Sb "bonds" are drawn as gray cylinders.

(note that, for simplicity, the defects on the In sites are not considered here) with Na^+ cations filling the channels within it. Figure 5b depicts the structure of $Na_{15}Ca_3In_5Sb_{12}$, where the Na−Sb bonds (tetrahedral ones) are shown to guide the eye, as well as the bonds between In and Sb (differentiated in light blue). By comparing the two images, one can see that $Na_{15}Ca_3In_5Sb_{12}$, reformulated as $Na_9Ca_3(In_5Na_6)Sb_{12}$, or notwithstanding the defects on the In site as $(Na_{0.75}Ca_{0.25})(In_{0.5}Na_{0.5})Sb$, is a variant of the same structure; the "coloring" of the atomic positions describing the framework is different. Figure 5c shows $Na_4CaGaSb_3$ drawn in a similar manner [can be reformulated as $Na_2Ca(GaNa_2)Sb_3$, or rather $(Na_{0.67}Ca_{0.33})(Ga_{0.33}Na_{0.67})Sb$]. Figure 5d is a representation of the

DOI: 10.1021/ic502822v
Inorg. Chem. 2015, 54, 1931−1939

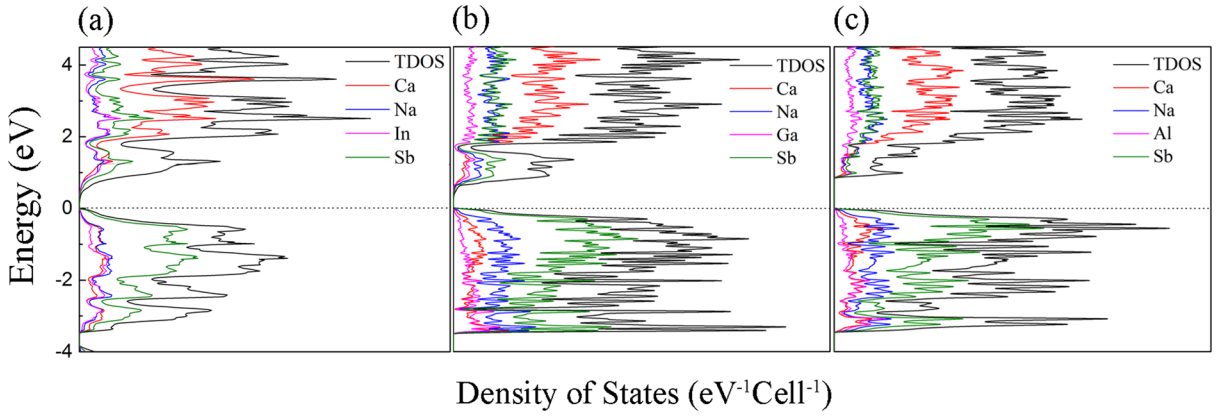

Figure 6. Calculated total and partial DOS curves for $Na_{15}Ca_3In_5Sb_{12}$ (a), $Na_4CaGaSb_3$ (b), and $Na_{11}Ca_2Al_3Sb_8$ (c). The Fermi level is the energy reference at 0 eV.

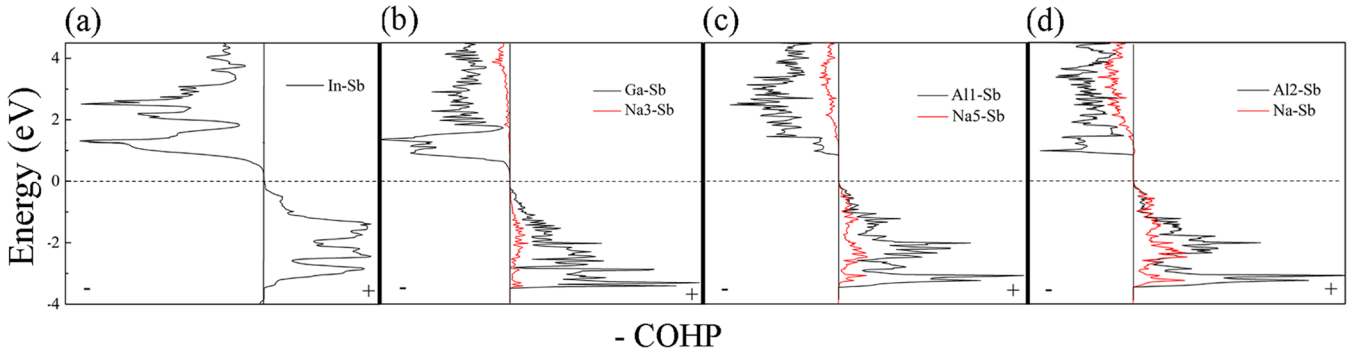

Figure 7. COHP curves for In−Sb, Ga−Sb, and Al−Sb (black lines) and for selected Na−Sb interactions (red lines). Panel a refers to $Na_{15}Ca_3In_5Sb_{12}$, panel b refers to $Na_4CaGaSb_3$, and panels c and d refer to $Na_{11}Ca_2Al_3Sb_8$. In plots of the COHP curves, the COHP values were inverted (i.e., −COHP is shown) so that the positive and negative regions represent bonding and antibonding states, respectively. The Fermi level is the energy reference at 0 eV.

$Na_{11}Ca_2Al_3Sb_8$ structure, where the relationship to the "parent" is the most complicated among all three, yet composing similar Al−Na−Sb hybrid layers allows for the structure to be viewed as $Na_6Ca_2(Al_3Na_5)Sb_8$, or $(Na_{0.75}Ca_{0.25})(Al_{0.375}Na_{0.625})Sb$ if normalized to the 1:1:1 stoichiometry. Note also that, for ease of viewing, the ordering of the Na and Ca atoms filling the channels (in all cases) has been exaggerated.

Electronic Structure. The calculated DOS are presented in Figure 6; the COHPs for selected atom pairs are projected in Figure 7. For all three structures, idealized models were considered, whereby the mixed-occupied Na/Ca positions were treated as either Na or Ca, and then the Fermi level was adjusted to the correct number of valence electrons per formula unit. For $Na_{15}Ca_3In_5Sb_{12}$, where in addition to the Na/Ca disorder partial occupancy on the In site is also observed (vide supra), we used the idealized, stoichiometric formula $Na_2CaInSb_2$ (as in the archetype $K_2BaCdSb_2$[26]) and then integrated the DOS for the experimental number of valence electrons and placed the Fermi level accordingly.

As shown in Figure 6, the DOS plot of $Na_{15}Ca_3In_5Sb_{12}$ is much simpler than those of $Na_4CaGaSb_3$ and $Na_{11}Ca_2Al_3Sb_8$, which is apparently due to the greater complexity of the latter two structures. As discussed before, there are only six unique atoms in the asymmetric unit of the $Na_{15}Ca_3In_5Sb_{12}$ structure, while $Na_4CaGaSb_3$ and $Na_{11}Ca_2Al_3Sb_8$ have nearly three times as many. Notwithstanding the differences in the general appearance of the curves, one can notice that there is a small energy gap between the top of the valence band and the bottom of the conduction band, which indicates small-gap semiconductor properties. Compared with that, the band gap in $Na_4CaGaSb_3$ is larger, as expected for a compound with the less electronegative Ga (χ_{Ga} = 1.6; χ_{In} = 1.7 on the Pauling scale[30]). Similarly, the band gap widens a bit more for $Na_{11}Ca_2Al_3Sb_8$ (χ_{Al} = 1.5 on the Pauling scale[30]). Such a comparison of the calculated band gaps, of course, should be taken with caution because the three compounds under consideration are not isotypic and there are marked differences in their structures. We also need to acknowledge the relatively small amount of the Tr element in the structures and the fact that Sb and Na/Ca electronic states dominate on both sides of the band gap; in that sense, the notion that the choice of the Tr element will strongly influence the size of the band gap can be easily refuted. The calculated band gaps vary from 0.05 to 0.75 eV, which could mean that some of these compounds (or their properly designed solid solutions) could be potentially good thermoelectric materials, a speculation that comes about from recognizing that similar antimonide compounds are well-known as high-efficiency thermoelectric materials.[6−8]

The states just below the Fermi levels in $Na_{15}Ca_3In_5Sb_{12}$ are predominately from the contribution of the Sb 5p orbital. Judging from the COHPs, the contribution from the Ca and Na states is limited, which means their roles are largely of electron donors, as in the classical Zintl description. This is not quite true for $Na_4CaGaSb_3$ and $Na_{11}Ca_2Al_3Sb_8$, where the Sb 5p states still have the major contribution; however, the relative contributions from Na and Ca to the total DOS appear to

DOI: 10.1021/ic502822v
Inorg. Chem. 2015, 54, 1931−1939

increase. Given that there are Na/Ca atoms in tetrahedral voids (recall the interlayer Na vs intralayer Na atoms; Figure 3), the implied higher degree of covalence is not difficult to understand. We can relate this finding to the previously published $Ba_2Cd_2Sb_3$[39] and Ba_2ZnSb_2,[5] for example, in which the Ba atoms, despite their very low electronegativity (χ_{Ba} = 0.9 on the Pauling scale[30]), also have important contributions to the DOS near the Fermi levels.

Last, we turn our attention to the COHP plots for $Na_{15}Ca_3In_5Sb_{12}$, $Na_4CaGaSb_3$, and $Na_{11}Ca_2Al_3Sb_8$ presented in Figure 7. From the graphs, it can be surmised that all In−Sb, Ga−Sb, and Al−Sb interactions are fully optimized at the Fermi level. This is expected because optimization of the interactions (at least within the anionic substructure) is a typical feature of the classic Zintl compounds. Considering the Na−Sb interactions involving the intralayer Na atoms, it becomes obvious that, for both $Na_4CaGaSb_3$ and $Na_{11}Ca_2Al_3Sb_8$, the Na−Sb bonding states are also filled at the Fermi level; i.e., the bonding is again optimized. Compared with the Ga−Sb and Al−Sb COHPs, however, it is noticeable that the Na−Sb interactions are much weaker. For instance, in $Na_4CaGaSb_3$, the integrated COHPs of the Na−Sb bonds (within the Na2 tetrahedra) range from 0.024 to 0.036, more than 5 times smaller than the integrated COHPs of the Ga−Sb bonds, which range from 0.143 to 0.217.

CONCLUSIONS

The three new compounds $Na_{15}Ca_3In_5Sb_{12}$, $Na_4CaGaSb_3$, and $Na_{11}Ca_2Al_3Sb_8$ are the first structurally characterized phases in the respective quaternary Na−Ca−Tr−Sb systems (Tr = Al, Ga, In). Their structures boast different structure types and feature the following: two-dimensional $[InSb_2]$ layers in $Na_{15}Ca_3In_5Sb_{12}$; one-dimensional $[GaSb_3]$ helical chains in $Na_4CaGaSb_3$. In the $Na_{11}Ca_2Al_3Sb_8$ structure, one finds isolated $[Al_3Sb_8]$ trimeric species. All three structures are related to the ubiquitous TiNiSi structure type. The study of the close structural relationships is greatly facilitated by considering some of the Na atoms in ambivalent roles, i.e., as contributing to the covalent bonding and forming complex Na−Al−Sb and Na−Ga−Sb slabs. The computed electronic structures show narrow band gaps at the Fermi level, suggesting that the title compounds could be considered as Zintl phases. The band gaps open in order of reduced dimensionality on the order from the In to the Ga to the Al compound. The expected intrinsic semiconducting properties could be of relevance to the development of new thermoelectric materials.

ASSOCIATED CONTENT

Supporting Information

X-ray crystallographic files in CIF format, additional details of the structural work, and figures showing structural representations with anisotropic displacement parameters and other structural relationships. This material is available free of charge via the Internet at http://pubs.acs.org.

AUTHOR INFORMATION

Corresponding Author

*E-mail: bobev@udel.edu. Phone: (302) 831-8720. Fax: (302) 831-6335.

Author Contributions

The manuscript was written through contributions of all authors. All authors have given approval to the final version of the manuscript.

Notes

The authors declare no competing financial interest.

ACKNOWLEDGMENTS

S.B. gratefully acknowledges financial support from the U.S. Department of Energy, Basic Energy Sciences, through Grant DE-SC0008885. We thank N.-T. Suen for discussions and help with the electronic structure calculations.

REFERENCES

(1) Schäfer, H.; Eisenmann, B.; Muller, W. *Angew. Chem., Int. Ed. Engl.* **1973**, *12*, 694−712. (b) Corbett, J. D. *Angew. Chem., Int. Ed.* **2000**, *39*, 670−690.
(2) (a) Kauzlarich, S. M., Ed. *Chemistry, Structure and Bonding in Zintl Phases and Ions*; VCH: New York, 1998; and references cited therein. (b) Miller, G. J. *Eur. J. Inorg. Chem.* **1998**, 523−536.
(3) Xia, S.-Q.; Bobev, S. *Inorg. Chem.* **2008**, *47*, 1919−1921.
(4) Xia, S.-Q.; Bobev, S. *J. Am. Chem. Soc.* **2007**, *129*, 4049−4057.
(5) Saparov, B.; Bobev, S. *Inorg. Chem.* **2010**, *49*, 5173−5179.
(6) Brown, S. R.; Kauzlarich, S. M.; Gascoin, F.; Snyder, G. J. *Chem. Mater.* **2006**, *18*, 1873−1877.
(7) Sales, B. C.; Mandrus, D.; Williams, R. K. *Science* **1996**, *272*, 1325−1328.
(8) Gascoin, F.; Ottensmann, S.; Stark, S.; Haïle, S. M.; Snyder, G. J. *Adv. Funct. Matter.* **2005**, *15*, 1860−1864.
(9) Andersen, O. K. *Phys. Rev. B: Condens. Matter* **1975**, *12*, 3060−3083.
(10) Villars, P., Calvert, L. D., Eds. *Pearson's Handbook of Crystallographic Data for Intermetallic Compounds*, 2nd ed.; American Society for Metals: Materials Park, OH, 1997.
(11) Wang, Y.; Bobev, S. Unpublished results. The corresponding CIF is provided as SI.
(12) Cordier, G.; Schäfer, H.; Stelter, M. *Z. Naturforsch.* **1985**, *B40*, 5−8.
(13) Cordier, G.; Ochmann, H. *Z. Kristallogr.* **1991**, *195*, 107−108.
(14) Deller, K.; Eisenmann, B. *Z. Naturforsch.* **1976**, *B31*, 29−34.
(15) Cromer, D. T. *Acta Crystallogr.* **1959**, *12*, 41−45.
(16) (a) *SMART*; Bruker AXS Inc.: Madison, WI, 2003. (b) *SAINT*; Bruker AXS Inc.: Madison, WI, 2003.
(17) *SADABS*; Bruker AXS Inc.: Madison, WI, 2003.
(18) *SHEXLTL*; Bruker AXS Inc.: Madison, WI, 2003.
(19) Jepsen, O.; Burkhardt, A.; Andersen, O. K. *The TB-LMTO-ASA Program*, version 4.7; Max-Planck Institut für Festkörperforschung: Stuttgart, Germany, 1999.
(20) Andersen, O. K.; Jepsen, O. *Phys. Rev. Lett.* **1984**, *53*, 2571−2574.
(21) Andersen, O. K.; Pawlowska, Z.; Jepsen, O. *Phys. Rev. B: Condens. Matter* **1986**, *34*, 5253−5269.
(22) Dronskowski, R.; Blöchl, P. E. *J. Phys. Chem.* **1993**, *97*, 8617−8624.
(23) Barth, U.; Hedin, L. *J. Phys. C: Solid State Phys.* **1972**, *5*, 1629−1642.
(24) Andersen, O. K.; Jepsen, O.; Glötzel, D. In *Highlights of Condensed Matter Theory*; Bassani, F., Fumi, F., Tosi, M., Eds.; North-Holland: New York, 1985.
(25) Blöchl, P. E.; Jepsen, O.; Andersen, O. K. *Phys. Rev. B: Condens. Matter* **1994**, *49*, 16223−16233.
(26) Saparov, B.; Saito, M.; Bobev, S. *J. Solid State Chem.* **2011**, *184*, 432−440.
(27) The one-electron difference between Cd and In, while maintaining an ideal valence electron count, is compensated for by defects on the In site and the concomitant nearly equal cooccupation by Ca and Na on one of the cation sites. See the SI for further details.

DOI: 10.1021/ic502822v
Inorg. Chem. 2015, 54, 1931−1939

(28) Xia, S.-Q.; Bobev, S. *Chem.—Asian J.* **2007**, *2*, 619−624.
(29) Cordier, G.; Schäfer, H.; Stelter, M. *Z. Naturforsch.* **1985**, *B40*, 858−871.
(30) Pauling, L. *The Nature of the Chemical Bond*; Cornell University Press: Ithaca, NY, 1960.
(31) The integrated COHP values nicely correlate with the bond distances. For example, for the shortest Ga1−Sb1 bond, the integrated COHP value is calculated to be 0.217. Considering Ga2, the Ga2−Sb5 bond is comparably short and has an integrated COHP value of 0.211. The longer bonds are weaker, and their integrated COHP values are 0.143 for Ga1−Sb4 and 0.160 for Ga2−Sb4.
(32) Cordier, G.; Ochmann, H.; Schäfer, H. *Mater. Res. Bull.* **1986**, *21*, 331−336.
(33) *ICSD Database*; Fachinformationszentrum: Karlsruhe, Germany, 2014.
(34) Cordier, G.; Czech, E.; Jakowski, M.; Schäfer, H. *Rev. Chim.* **1981**, *18*, 9−18.
(35) Cordier, G.; Ochmann, H.; Schäfer, H. *Z. Anorg. Allg. Chem.* **1984**, *517*, 118−124.
(36) Saparov, B.; Xia, S.-Q.; Bobev, S. *Inorg. Chem.* **2008**, *47*, 11237−11244.
(37) Saparov, B.; Broda, M.; Ramanujachary, K. V.; Bobev, S. *Polyhedron* **2010**, *29*, 456−462.
(38) Bobev, S.; Sevov, S. C. *J. Solid State Chem.* **2001**, *163*, 436−448.
(39) Saparov, B.; He, H.; Zhang, X. H.; Greene, R.; Bobev, S. *Dalton Trans.* **2010**, *39*, 1063−1070.

DOI: 10.1021/ic502822v
Inorg. Chem. 2015, 54, 1931−1939